

# Deformation monitoring using Sentinel-1 SAR data

N. Devanthéry, M. Crosetto, O. Monserrat, M. Cuevas-González  
Geomatics Division,  
Centre Tecnològic de Telecomunicacions de Catalunya (CTTC) Av. Gauss, 7, E-08860 Castelldefels  
(Barcelona), Spain

B. Crippa  
Department of Earth Sciences,  
University of Milan, Via Cicognara 7, I-20129 Milan, Italy

**Abstract.** This paper describes the data processing and analysis procedure implemented by the authors to analyse Sentinel-1 data. The procedure is an advanced Differential Interferometric SAR (DInSAR) technique that generates deformation maps and time series of deformation from multiple SAR images acquired over the same site. The second part of the paper illustrates the results of the procedure. The first deformation monitoring results obtained using Sentinel-1 SAR data over the metropolitan area of Barcelona (Spain) are described and analysed.

**Keywords.** PSI, deformation monitoring, C-band, Sentinel-1.

## 1 Introduction

Satellite-based radar interferometry represents a powerful tool to detect and monitor ground deformation. Successful terrain deformation results have demonstrated the potential of this technique for a wide range of applications related for instance to landslides (Colesanti et al. (2003); Hilley et al. (2004); Bovenga et al. (2012)), land subsidence caused by groundwater pumping (Tomás et al. (2005); Stramondo et al. (2007); Bell et al. (2008); Heleno et al. (2011)), mining (Colesanti et al. (2005); Jung et al. (2007)) or urban planning (Crosetto et al. (2008); Vallone et al. (2008); Cigna et al. (2012)).

This paper is focused on the application of Persistent Scatterer Interferometry (PSI), see Ferreti et al. (2000, 2001), for land subsidence detection and measurement using the SAR data acquired by the Sentinel-1 satellite of the European Space Agency. DInSAR and PSI techniques have

experienced a major development in the last two decades (Crosetto et al. (2015)), which is mainly related to the progress accomplished through the exploitation of C-band data from ERS-1/2, Envisat and Radarsat. The data acquired by these satellites covers long periods of time, a key aspect to guarantee a long-term deformation monitoring. The advent of very high resolution X-band data in 2007 enabled a major step forward in the PSI techniques (Crosetto et al. (2015)), including the capability to generate a dense sampling of Persistent Scatterers (PSs), a higher sensitivity to small displacements and a remarkable quality improvement of the time series compared to the C-band. A new significant improvement is expected to occur thanks to the data acquired by the C-band sensor onboard the Sentinel-1 satellite. This satellite, launched on 3 April 2014, acquires interferometric C-band SAR data and offers an improved data acquisition capability with respect to previous C-band sensors (ERS-1/2, Envisat and Radarsat), increasing considerably the deformation monitoring potential. Sentinel-1 acquires images covering 250 by 180 km with a revisiting cycle of 12 days in its standard data acquisition mode (Interferometric Wide Swath). The revisiting cycle will become 6 days with the launch of the Sentinel-1b satellite. The Sentinel-1 coverage might be essential for certain applications that might benefit from a wide-area PSI monitoring using C-band Sentinel-1 data. Additionally, PSI analyses requires large image datasets, which are expensive to obtain with X-band sensors such as TerraSAR-X data, while with Sentinel-1 these data are freely available.

This article presents the authors' first PSI processing experience with Sentinel-1 data. The processing strategy is described and the first results obtained over the metropolitan area of Barcelona are illustrated.

## 2 Methodology

A set of  $N$  images and a redundant net of  $M$  interferograms are required to initiate the PSI procedure used in this work. The main processing steps (Devan  ry et al. (2014)) of the procedure are briefly described below:

- Atmospheric phase screen (APS) estimation and removal. A phase unwrapping is performed over the  $N-1$  consecutive interferograms, multi-looked 5 in range and 1 in azimuth to reduce the noise, covering the period of study. A direct integration, which consists in retrieving the images phases with respect to a given image, is then carried out over the unwrapped interferograms. Finally, the APS estimation is performed by means of a set of spatio-temporal filters (Ferreti et al. (2000, 2001); Berardino et al. (2002); Mora et al. (2003)) and removed from the original interferograms at full resolution.
- Deformation velocity and residual topographic error (RTE) estimation. The deformation velocity and RTE are computed over a set of PSs, from the  $M$  wrapped APS-free interferograms, using the method of the periodogram. Optionally, an extension of the two-parameter model can be used to account for the thermal expansion (Monserrat et al. (2011)).
- RTE removal. The RTE phase component is removed from the wrapped APS-free interferograms. The linear deformation component can optionally be removed and then, in a later stage, added back to the deformation time series. The same procedure can be done with the thermal expansion component. Note that this step is required to correctly estimate the accumulated deformation and time series in the 2+1D phase unwrapping stage, in which the interferometric phases need to be APS-free and RTE-free to avoid confusing the deformation with other components, as well as to avoid phase unwrapping errors due to phase gradients related to RTE. This is especially important when performing measurements in urban areas.
- 2+1D phase unwrapping. This is the key step of the procedure, where the accumulated deformation map and the time series are derived from the redundant network of interferograms free of APS and RTE at full resolution. A spatial 2D phase unwrapping is performed separately on each interferogram using the

Minimum Cost Flow method (Costantini (1998); Costantini et al. (1999)). Following this step, a 1D phase unwrapping is performed pixel wise over the  $M$  interferograms. This last step is able to detect and correct the errors generated during the 2D phase unwrapping stage, and provides tools to control the quality of the derived time series. For this purpose, an iterative LS procedure (Baarda (1968); Bj  rck (1996); F  rstner (1986)) which fully exploits the integer nature of the unwrapping errors is used. It is based on the estimation of the following system of equations:

$$\begin{aligned}\Delta\varphi_{MS} &= \varphi_S - \varphi_M \\ \tilde{\varphi}_0 &= 0\end{aligned}\quad (1)$$

where  $\Delta\varphi_{MS}$  is the unwrapped interferometric phase (the observation),  $S$  and  $M$  are the slave and master images and  $\varphi_S$  and  $\varphi_M$  are the corresponding unknown phases. The phase of the first image  $\varphi_0$  is set to zero. The system is solved by means of an iterative LS driven by two key parameters: the residuals  $\tilde{\varphi}_{res}$  and the redundancy of the network.

## 3 Results

19 Interferometric Wide (IW) Single Look Complex (SLC) Sentinel-1 images have been used to derive the deformation measurements. An IW SLC Sentinel-1 scene covers approximately 250 x 180 km and is composed of three swaths containing nine bursts each.

In this study, the PSI procedure is performed burst-wise over the interferograms at full resolution, i.e., with a footprint of approximately 5 x 20 m in range and azimuth, respectively. In this study, we focus on the results over the burst 9 of the swath 1. The main PSI products are the accumulated deformation map and the time series of the deformation derived from the set of 19 images, spanning the period from March to December 2015, and using a redundant network of 171 interferograms with perpendicular baselines ranging from -146 m to 208 m.

The accumulated deformation map was estimated over an area of approximately 1250 km<sup>2</sup> in the northern metropolitan area of Barcelona, including some countryside areas (see Figure 1). The area

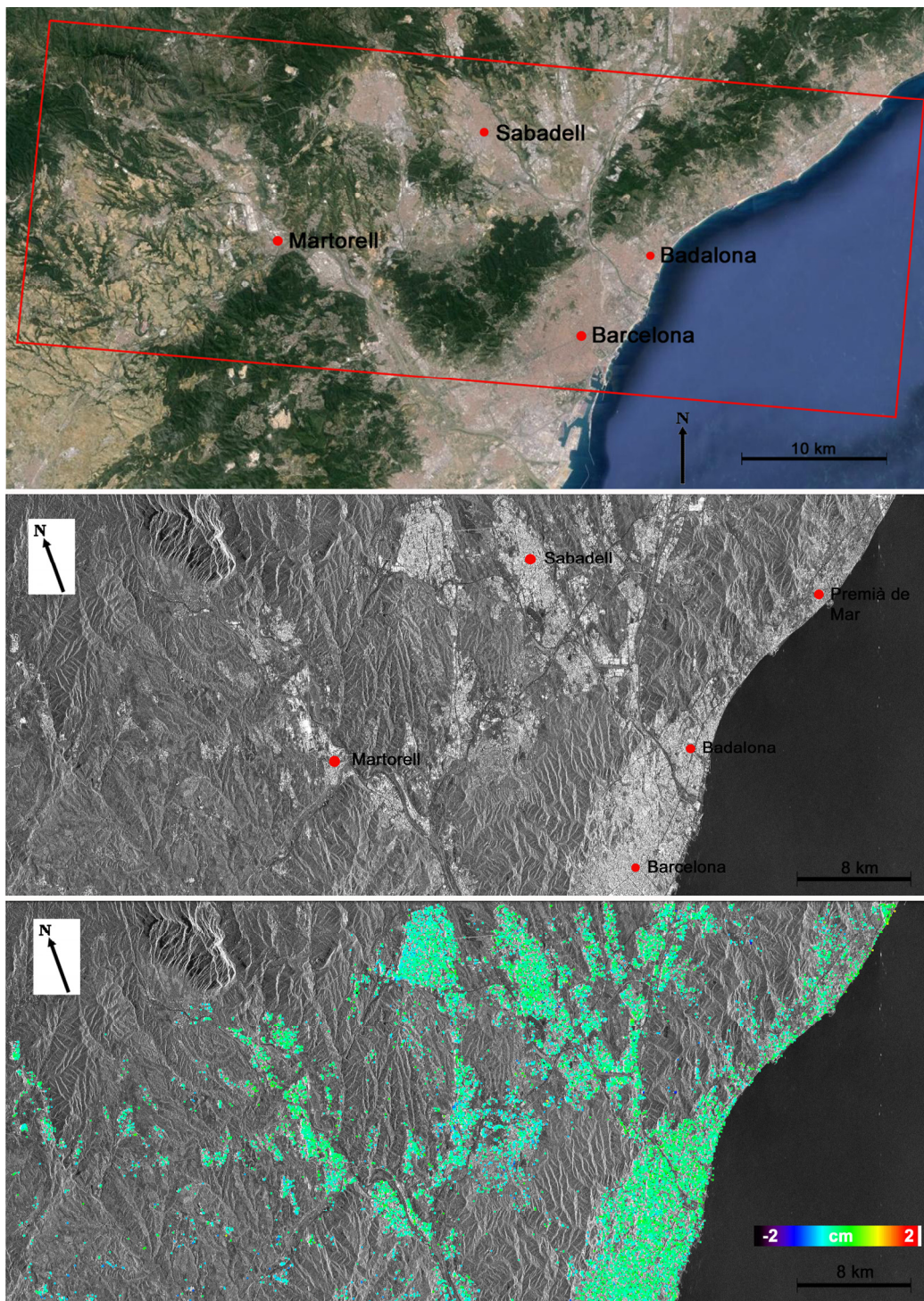


**Fig. 1** *Top*: Google Earth orthoimage of the studied area (red rectangle). *Middle*: SAR amplitude of the burst 9 of swath 1 of Catalonia dataset acquired by the Sentinel-1 satellite. *Bottom*: accumulated deformation map superimposed on the mean amplitude image.



limited by the red rectangle in Figure 1 shows the study area, i.e. the area comprised in the burst 9 of swath 1. The middle image in Figure 1 shows the mean amplitude of the 19 SAR images over the same area in radar geometry, while the image at the bottom is the accumulated deformation map superimposed on the mean amplitude image. The deformation measurements were derived for a total of 104861 PSs, covering and connecting all the urban areas of the scene (see image at the bottom of Figure 1).

Positive values (red) indicate displacements away from the sensor, while the negative ones (blue) denote displacements toward the SAR sensor. Note that these values refer to the SAR Line-of-Sight (LOS). Although most of the area in the scene is stable (green points), some terrain displacement have been found. However, a further densification of PS is required to allow a detailed analysis of the deformations.

Sentinel-1 SAR imagery offers wide-area coverage associated to a relatively high spatial resolution, therefore allowing to obtain a comprehensive outlook of the deformation phenomena occurring in wide areas while, at the same time, maintaining the capability to measure individual features such as buildings or infrastructures. It is also important to note that the PSI technique is opportunistic, which means that it is only able to estimate deformation over those points where PSI phases maintain good quality over time to get reliable deformation estimates.

Figure 2 shows the PS density over the city of Barcelona. The density found in this urban area is 390 PS/km<sup>2</sup>, which is a good density considering that the IW SLC Sentinel-1 pixel resolution is about 5 x 20 m in azimuth and range, respectively.

The deformation time series is one of the most interesting and advanced products derived from the PSI procedure. Figure 3 shows three time series with different behaviors, which illustrate the sensibility and precision of the measurements: a subsidence of up to 20 mm during the 9 months of observations (circles), an uplift reaching 15 mm (diamonds) probably caused by the interruption of water pumping, and a rather stable PS which has been included in order to show the quality of the results (squares). Note that the time series are slightly noisy, probably due to the small number of images available to perform the processing and the short period of time analyzed.



Fig. 2 Example of the PS sample density achieved in the urban area of the processed burst.

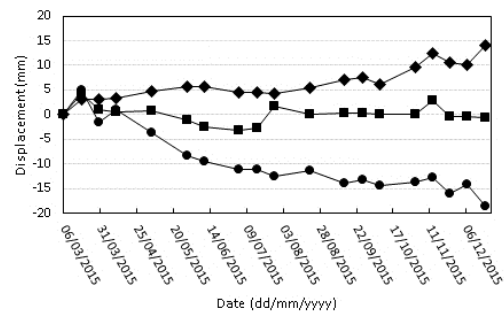


Fig. 3 Example of deformation time series.

## 4 Conclusions

The first results obtained by the authors' from Sentinel-1 images using PSI techniques have been presented. A brief description of the processing chain has been provided, followed by an analysis of the results achieved over the burst covering the northern metropolitan area of Barcelona: The deformation map and time series of deformation over an approximate area of 1250 km<sup>2</sup>, with a density of 390 PS/km<sup>2</sup> in urban areas, have been shown.

The next step of the procedure will be to perform the analysis for the entire scene, i.e. the 9 bursts of the 3 swaths of the IW SLC Sentinel-1 scene. The goal is to derive the deformation map over the region of Catalonia, performing local densification when required to study any given deformation phenomena.

## References

- Baarda, W. (1968). A Testing Procedure for Use in Geodetic Networks; Kanaalweg 4, *Rijkscommissie voor Geodesie*: Delft, The Netherlands.
- Berardino, P., Fornaro, G., Lanari, R., and Sansosti, E. (2002). A new algorithm for surface deformation monitoring based on small baseline differential SAR interferograms. *IEEE Trans. Geosci. Remote Sens.*, 40, 11, 2375–2383.
- Bell, J.W., Amelung, F., Ferretti, A., Bianchi, M., Novali, F. (2008). Permanent scatterer InSAR reveals seasonal and longterm aquifer-system response to groundwater pumping and artificial recharge, *Water Resour. Res.*, 44, W02407, doi:10.1029/2007WR006152.
- Björck, Å. (1996). Numerical Methods for Least Square Problems; *Siam*: Philadelphia, PA, USA.
- Bovenga, F., Wasowski, J., Nitti, D.O., Nutricato, R., Chiaradia, M.T. (2012). Using COSMO/SkyMed X-band and ENVISAT Cband SAR interferometry for landslides analysis, *Remote Sens. Environ.*, 119, pp. 272–285.
- Cigna, F., Osmanoglu, B., Cabral-Cano, E., Dixon, T.H., Ávila-Olivera, J.A., Garduño-Monroy, V.H., DeMets, C., Wdowinski, S. (2012). Monitoring land subsidence and its induced geological hazard with Synthetic Aperture Radar Interferometry: A case study in Morelia, Mexico, *Remote Sens. Environ.*, 117, pp. 146–161.
- Colesanti, C., Ferretti, A., Prati, C., and Rocca, F. (2003). Monitoring landslides and tectonic motions with the Permanent Scatterers Technique, *Eng. Geol.*, 68, pp. 3–14.
- Colesanti, C., Le Mouélic, S., Bennani, M., Raucoules, D., Carnec, C. and Ferretti, A. (2005). Detection of mining related ground instabilities using the permanent scatterers technique - a case study in the east of France, *Int. J. Remote Sens.*, 26(1), pp. 201–207.
- Costantini, M. (1998). A novel phase unwrapping method based on network programming, *IEEE Trans. Geosci. Remote Sens.*, 36, pp. 813–821.
- Costantini, M., Farina, A., Zirilli, F. (1999). A fast phase unwrapping algorithm for SAR interferometry, *IEEE Trans. Geosci. Remote Sens.*, 37, pp. 452–460.
- Crosetto, M., Biescas, E., Duro, J., Closa, J., Arnaud, A. (2008). Generation of Advanced ERS and Envisat Interferometric SAR Products Using the Stable Point Network Technique, *Photogramm. Eng. Rem. S.*, 74(4), pp. 443–450.
- Crosetto, M., Monserrat, O., Cuevas-González, M., Devanthery, N. (2015). Persistent Scatterer Interferometry: a review. *Accepted in ISPRS J. of Photogrammetry and Remote Sensing*.
- Devanthery, N., Crosetto, M., Monserrat, O., Cuevas-González, M., and Crippa, B. (2014). An approach to Persistent Scatterer Interferometry, *Remote Sensing*, 6(7), pp. 6662–6679.
- Ferretti, A., Prati, C., Rocca, F. (2000). Nonlinear subsidence rate estimation using permanent scatterers in differential SAR interferometry. *IEEE Trans. Geosci. Remote Sens.*, 47(5), pp. 2202–2212.
- Ferretti, A., Prati, C., Rocca, F. (2001). Permanent scatterers in SAR interferometry, *IEEE Trans. Geosci. Remote Sens.*, 39(1), pp. 8–20.
- Förstner, W. (1986). Reliability, gross error detection and self-calibration, *ISPRS Commission III Tutorial on Statistical Concepts for Quality Control. ISPRS Int. Arch. Photogramm.*, 26, pp. 1–34.
- Heleno, S.I.N., Oliveira, L.G.S., Henriques, M.J., Falcão, A.P., Lima, J.N.P., Cooksley, G., Ferretti, A., Fonseca, A.M., Lobo-Ferreira, J.P., Fonseca, J.F.B.D. (2011). Persistent Scatterers Interferometry detects and measures ground subsidence in Lisbon, *Remote Sens. Environ.*, 115, pp. 2152–2167.
- Hilley, G. E., Bürgmann, R., Ferretti, A., Novali, F., and Rocca, F. (2004). Dynamics of slow-moving landslides from Permanent Scatterer analysis, *Science*, 304 (5679), pp. 1952–1955.
- Jung, H., Kim, S., Jung, H., Min, K., Won, J. (2007). Satellite observation of coal mining subsidence by permanent scatterer analysis, *Eng. Geol.*, 92, pp. 1–13.
- Monserrat, O., Crosetto, M., Cuevas, M., Crippa, B., (2011). The thermal expansion component of Persistent Scatterer Interferometry observations, *IEEE Geosci. Remote Sens. Letters*, 8, pp. 864–868.
- Mora, O., Mallorquí, J.J., and Broquetas, A. (2003). Linear and nonlinear terrain deformation maps from a reduced set of interferometric SAR images. *IEEE Trans. Geosci. Remote Sens.*, 41, 10, 2243–2253.
- Stramondo, S., Saroli, M., Tolomei, C., Moro, M., Doumaz, F., Pesci, A., Loddo, F., Baldi, P., Boschi, E. (2007). Surface movements in Bologna (Po Plain – Italy) detected by multitemporal DInSAR, *Remote Sens. Environ.*, 110, pp. 304–316.
- Tomás, R., Márquez, Y., Lopez-Sanchez, J.M., Delgado, J., Blanco, P., Mallorquí, J.J., Martínez, M., Herrera, M., Mulas, J. (2005). Mapping ground subsidence induced by aquifer overexploitation using advanced Differential SAR interferometry: Vega Media of the Segura river (SE Spain) case study, *Remote Sens. Environ.*, 98, pp. 269–283.
- Vallone, P., Giammarinaro, M. S., Crosetto, M., Agudo, M., Biescas, E. (2008). Ground motion phenomena in Caltanissetta (Italy) investigated by InSAR and geological data integration, *Eng. Geol.*, 98, pp. 144–155.